Received 7 July 2008
Revised 25 February 2009
Accepted 6 April 2009

Predicting uncertainty and confidence intervals in thermal radiative modeling using the Monte Carlo ray-trace method

María Cristina Sánchez
Department of Mechanical Engineering, California State University, Fresno, California, USA, and
J.R. Mahan
(Formerly) Department of Mechanical Engineering, Virginia Polytechnic Institute and State University, Blacksburg, Virginia, USA

Abstract

Purpose – The purpose of this paper is to present the results obtained from numerical models of radiant energy exchange in instruments typically used to measure various characteristics of the Earth's ocean-atmosphere system.

Design/methodology/approach – Numerical experiments were designed and performed in a statistical environment, based on the Monte Carlo ray-trace (MCRT) method, developed to model thermal and optical systems. Results from the derived theoretical equations were then compared to the results from the numerical experiments.

Findings – A rigorous statistical protocol is defined and demonstrated for establishing the uncertainty and related confidence interval in results obtained from MCRT models of radiant exchange.

Research limitations/implications – The methodology developed in this paper should be adapted to predict the uncertainty of more comprehensive parameters such as the total radiative heat transfer.

Practical implications – Results can be used to estimate the number of energy bundles necessary to be traced per surface element in a MCRT model to obtain a desired relative error.

Originality/value – This paper offers a new methodology to predict the uncertainty of parameters in high-level modeling and analysis of instruments that accumulate the long-term database required to correlate observed trends with human activity and natural phenomena. The value of this paper lies in the interest in understanding the climatological role of the Earth's radiative energy budget.

Keywords Modeling, Thermal measurement, Oceans, Atmosphere, Climatology, Heat transfer
Paper type Research paper

Nomenclature

Symbols

A	area (m^2)
D'_{ij}	distribution factor from surface i to surface j
E	estimated value
Err	error
n	number of surfaces
N	number of energy bundles
P	power (W)
q″	net heat flux (W/m^2)
Q	radiative energy (W)
r_s	specularity ratio
R	uniformly distributed random number between zero and unity
s	standard deviation
T	temperature (K)
W	W-statistic

International Journal of Numerical Methods for Heat & Fluid Flow
Vol. 20 No. 1, 2010
pp. 66-83

0961-5539
DOI 10.1108/09615531011008127

Greek

α	absorptivity	$\omega_{K\&M}$	uncertainty obtained using the Kline and McClintock formalism
ε	emissivity	ω_{exp}	experimental uncertainty
ρ	reflectivity		
σ	Stefan-Boltzmann constant (W/m^4)		

1. Introduction

Monte Carlo methods have been used for a number of years in a wide variety of areas of interest to the scientific and engineering communities. In particular, application of Monte Carlo ray-trace (MCRT) method to heat transfer problems has grown rapidly since its use was first reported in the 1960s. In what appears to be the first publication describing the Monte Carlo approach to radiation heat transfer, Howell and Perlmutter (1964) describe a method to calculate the heat transfer and temperature distribution between infinite parallel gray plates at different temperatures separated by an absorbing and emitting gray gas with or without a uniform heat source in the gas. Later in 1966 Corlett (1966) used the Monte Carlo method to develop a program intended for engineering calculation of thermal radiation in real enclosures. In the same year, Sparrow and Cess (1966) briefly discussed the application of Monte Carlo methods in thermal radiation problems. The MCRT method has subsequently proven to be very useful in the estimation of the diffuse-specular distribution factor D'_{ij}[1] (Mahan and Eskin, 1984) used, for example, in various radiometric instrument models. In this approach radiation energy is modeled as a large number of individual energy bundles that are traced inside an enclosure from their origin until they are absorbed by a surface of the enclosure. The diffuse-specular radiation distribution factor[1] may be estimated as

$$D'_{ij} \cong \frac{N_{ij}}{N_i} \tag{1}$$

where N_i is the number of energy bundles emitted from surface element i and N_{ij} is the number of these energy bundles absorbed by surface element j. The radiation distribution factor may be defined for a specific wavelength interval $\Delta\lambda$ or it may be a "total" quantity if conditions permit a "gray" analysis.

Consistent with the definition of the diffuse-specular distribution factor, the heat (W) emitted by surface element i and absorbed by surface element j is given by

$$Q_{ij} = \varepsilon_i A_i \sigma T_i^4 D'_{ij} (W) \tag{2}$$

where ε_i and A_i are the emissivity and area of surface element i, and σ is the Stefan-Boltzmann constant ($= 5.67 \times 10^{-8}$ $W/m^2 \cdot K^4$). Then the heat flux absorbed by surface element i is

$$q''_{i,a} = \frac{Q_{i,a}}{A_i} = \frac{1}{A_i} \sum_{j=1}^{n} \varepsilon_j A_j \sigma T_j^4 D'_{ji} = \varepsilon_i \sum_{j=1}^{n} \sigma T_j^4 D'_{ij} \ (W/m^2) \tag{3}$$

In writing Equation (3) the principle of reciprocity for the total, diffuse-specular distribution factor, $\varepsilon_i A_i D'_{ij} = \varepsilon_j A_j D'_{ij}$, has been used (Mahan and Eskin, 1984). The radiation heat flux emitted by surface element i is

$$q''_{i,e} = \frac{Q_{i,e}}{A_i} = \varepsilon_i \sigma T_i^4 \ (W/m^2) \tag{4}$$

Then the net heat flux from surface element i is

$$q''_i = q''_{i,e} - q''_{i,a} = \sum_{j=i}^{n} \varepsilon_i \sigma T_j^4 (\delta_{ij} - D'_{ij}), \ i = 1, 2, 3, \ldots, n \tag{5}$$

where δ_{ij} is the Kronecker delta,

$$\delta_{ij} = \begin{cases} 1, & i = j \\ 0, & i \neq j \end{cases} \tag{6}$$

2. Uncertainty and confidence interval for thermal radition distribution factors

The basic idea of treating the exchange fraction of energy (modeled as discrete energy bundles) between two surfaces as a series of independent Bernoulli trials was first seen by the current author in a publication by Maltby and Burns (1991). However, the current author considered the statistical inferences to be incomplete for this application and decided to pursue an independent development. In Maltby, the parameter (standard deviation) is defined for the population distribution, while in the current paper it was necessary to describe the parameter for the sample distribution. Also, the previous effort only looked at the uncertainty of a single exchange factor and its relation to the magnitude of the exchange factor and the number of emitted energy bundles, while the current effort also investigates a global uncertainty of the entire cavity and its sensitivity to the number of surfaces (spatial discretization) in the cavity.

Koopmans (1987) defines the population proportion as the probability of "success" in a binomial experiment (e.g. the number of heads in repeated coin tosses). In other words, if Y is a binomial variable, the population proportion π is the probability of obtaining one of the two possible outcomes of the experiment. Sometimes it is important to know not only the variable Y but also this variable divided by the sample size n. This new value is an estimator of the population proportion π. In the MCRT environment, the tracing of N_i energy bundles emitted by surface i can be considered a binomial experiment where "success" is achieved when one of the energy bundles is absorbed by the surface j. Accordingly, the diffuse-specular radiation distribution factor, which can be estimated using Equation (1), can be thought of as a sample proportion that estimates the value of the population proportion. As is the case in any proportion, the two possible outcomes in the ray trace are D'_{ij} and $1 - D'_{ij}$. It is important to note that the "true" value of the distribution factor is based on an infinite population of uniformly distributed random numbers while the estimate is based on a large but finite sample of this population.

Using the approach suggested above, the confidence interval for the binomial parameter D'_{ij}, the diffuse-specular distribution factor, can be estimated using the

expression

$$p - W_c s \leq D'_{ij} \leq p + W_c s \tag{7}$$

where p is an estimator of π, W_c is the critical value of the W statistic, and s is the estimated sample standard deviation given by

$$s = \sqrt{\frac{p(1-p)}{N}} \tag{8}$$

with N being the number of energy bundles traced. The W statistic for binomial distributions is tabulated in standard statistics texts as a function of the confidence interval and number of degrees of freedom.

Equation (7) can be written in terms of the estimated distribution factor

$$D'^{e}_{ij} - W_c \sqrt{\frac{D'^{e}_{ij}(1 - D'^{e}_{ij})}{N}} \leq D'^{t}_{ij} \leq D'^{e}_{ij} + W_c \sqrt{\frac{D'^{e}_{ij}(1 - D'^{e}_{ij})}{N}} \tag{9}$$

where now D'^{t}_{ij} is the (unknown) true value of the distribution factor and D'^{e}_{ij} is the MCRT estimate based on tracing N energy bundles. Subtracting D'^{e}_{ij} from each term of Equation (9) yields

$$-W_c \sqrt{\frac{D'^{e}_{ij}(1 - D'^{e}_{ij})}{N}} \leq D'^{t}_{ij} - D'^{e}_{ij} \leq W_c \sqrt{\frac{D'^{e}_{ij}(1 - D'^{e}_{ij})}{N}} \tag{10}$$

The magnitude of the difference between a true value and its estimated value can be defined as the error in the estimate. Equation (10) therefore provides a bound on the error of the estimate, which can be written as

$$Err_{D'_{ij}} \equiv |D'^{t}_{ij} - D'^{e}_{ij}| \leq W_c \sqrt{\frac{D'^{e}_{ij}(1 - D'^{e}_{ij})}{N}} = \omega_{D'_{ij}} \tag{11}$$

The bounds described in Equation (11) can be thought of as the uncertainty in the estimate of the distribution factor between surface i and j, $\omega_{D'_{ij}}$. In other words, to a stated level of confidence the absolute value of the error is limited by the uncertainty given by Equation (11).

It is useful to calculate the mean value of the error of all the radiation distribution factors in an enclosure. At this point, it is important to keep in mind that the radiation distribution factor matrix is obtained by modeling the emission of energy bundles from each surface in the cavity and counting the energy bundles absorbed in all of the surfaces. In this case

$$\langle\langle Err_{D'_{ij}} \rangle\rangle \equiv Err_{D'} \leq \left\langle \left\langle W_c \sqrt{\frac{D'^{e}_{ij}(1 - D'^{e}_{ij})}{N}} \right\rangle \right\rangle \tag{12}$$

Equation (12) can be evaluated using the Jensen's inequality (Beckenbach and Bellman,

1971) which states that for a real, continuous, convex function

$$E[f(x)] \geq f(E[x]) \quad \text{if f is concave upward} \tag{13}$$

and

$$E[f(x)] \leq f(E[x]) \quad \text{if f is concave downward} \tag{14}$$

where the expected value E is the mean value of the function f(x) over x. In other words

$$\frac{1}{M}\sum_{m=1}^{M} f(x_m) \geq f\left(\frac{1}{M}\sum_{m=1}^{M} x_m\right) \quad \text{if f is concave upward} \tag{15}$$

or

$$\frac{1}{M}\sum_{m=1}^{M} f(x_m) \leq f\left(\frac{1}{M}\sum_{m=1}^{M} x_m\right) \quad \text{if f is concave downward} \tag{16}$$

Now consider the definition o $\times$ f $Err_{D'} = f(D'^{e}_{ij})$in Equation (12). Figure 1 shows that this function is concave downward over the entire range of possible values for the distribution factors. Then the magnitude of the error of the distribution factors in Equation (12) is bounded according to

$$\omega_{D'} \leq W_c\sqrt{\frac{\langle\langle D'^{e}_{ij}\rangle\rangle(1 - \langle\langle D'^{e}_{ij}\rangle\rangle)}{N}} \tag{17}$$

Noting that $\langle\langle D'_{ij}\rangle\rangle = 1/n^2\sum_{i=1}^{n}\sum_{j=1}^{n} D'_{ij} = 1/n^2\sum_{i=1}^{n} 1 = 1/n$, with n being the number of surfaces in the enclosure, then Equation (17) gives

$$\omega_{D'} \leq W_c\sqrt{\frac{\frac{1}{n}(1 - \frac{1}{n})}{N}} \tag{18}$$

or

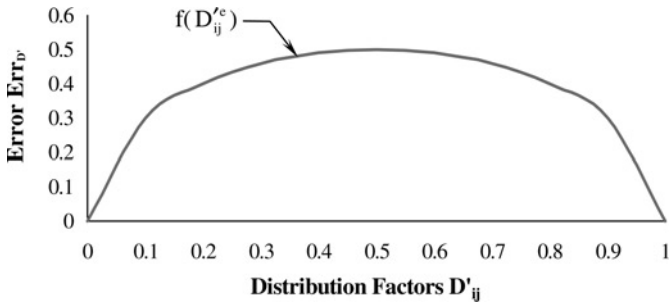

Figure 1.
Graphical representation of $W_c\sqrt{D'^{e}_{ij}(1 - D'^{e}_{ij})/N}$

$$Err_{D'} \leq \omega_{D'} \leq W_c \sqrt{\frac{n-1}{Nn^2}} \tag{19}$$

This is similar to the equation presented by Mahan (2002). However, the current work provides the rigorous development of the equation that is missing from the previous effort. Equation (19) provides an upper bound on the mean error and mean uncertainty of the distribution factors as a function of the number of surface elements, n, and the number of energy bundles traced per surface element N. It also can be used to calculate the minimum number of energy bundles that need to be traced to ensure that the error of the distribution factors is less than a specified value. It is emphasized that this result is independent of the enclosure geometry.

3. Cavity-type thermal radiation detector model

The possibility of anthropogenic modification of the Earth's climate has led to an increased interest in understanding the climatological role of the Earth's radiative energy budget. A series of major earth radiation budget (ERB) studies has been commissioned Barkstrom (1990) in an attempt to accumulate the long-term database required to correlate observed trends with human activity and natural phenomena. These include the National Aeronautics and Space Administration's (NASA) ongoing efforts to monitor the ERB using the Clouds and the Earth's Radiant Energy System (CERES) instrument (Wielicki *et al.*, 1996; Carman *et al.*, 1992), which provides broadband measurements of reflected solar and earth-emitted longwave radiances. These measurements are a continuation of the Earth Radiation Budget Experiment (ERBE) measurements (Barkstrom and Hall, 1982; Barkstrom and Smith, 1986) and are used in scientific investigations to determine top-of-the-atmosphere heat fluxes, radiative forcing properties of clouds, earth surface radiation budget, and divergence throughout the atmosphere. Due to the importance of these measurements to the scientific community, it is necessary to obtain a thorough understanding of the behavior of the instrument and the underlying physics governing that behavior. This can be achieved using detailed analytical models based on first principles of physics. High-level modeling and analysis of these instruments are essential to defining the accuracy of the data they produce, and it is of critical importance to have a thorough understanding of the accuracy and limitations of the models themselves.

The radiative behavior of the cavity-type thermal radiation detector described here and shown in Figure 2 has been reported elsewhere (Mahan *et al.*, 1998). This design was an instrument concept that was proposed for use on the Geostationary Earth Radiation Budget (GERB) experiment (Harries and Crommelynck, 1999; Harries *et al.*, 2005). Although the design was not used on GERB, it has been the object of several studies due to its simplicity and efficiency in directing incident radiation to the detector. A thermopile linear array is mounted on one of the nine mirror-like walls whose specular reflections increase the apparent absorptivity of the blackened array (Mahan and Langley, 1996). The linear array consists of 256 pixels. Each pixel is the darkened active junction of a two-junction thermopile. The incident collimated radiation enters the cavity through the 60-μm wide slit at the top and strikes the blackened active junction of each thermopile.

4. Windows-based MCRT program

Recently a colleague of the authors, Félix J. Nevárez, developed a statistical environment, based on the MCRT method, to model thermal and optical systems. This

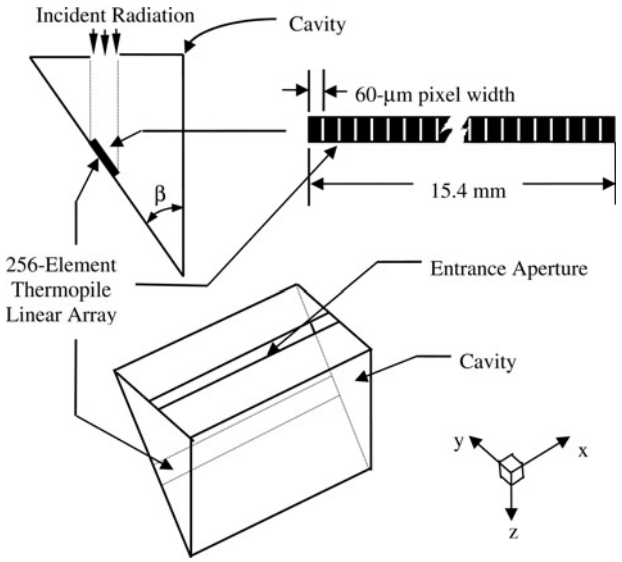

Figure 2.
Thermopile linear-array thermal radiation detector

powerful new tool, called Functional Environment for Longwave Infrared eXchange (FELIX), allows the user to model enclosures by importing an existing CAD rendering and assigning surface properties for a specific wavelength. A ray-trace engine is then used to calculate the distribution factors. The resulting distribution factors may be exported to a data file or viewed as false color maps through a graphical interface.

5. Results

The MCRT-based software package FELIX was used to model the cavity and to perform the majority of the numerical experiments described in this paper. Ten different numerical experiments, each one run with a different set of seeds for the pseudorandom number generator, have been studied. Each experiment consists of executing the ray trace for different numbers of energy bundles.

After defining the optical properties of the cavity and introducing the geometry in FELIX, the program yields the distribution factor matrix for the nine surfaces. Figure 3 illustrates the numbering of the surfaces of the cavity. For example, D_{61} is the distribution factor from the entrance aperture to the detector. Table I shows the values of the optical properties used in the ten experiments. The numerical experiments are used to establish the validity of Equations (11) and (19).

5.1 Validation of Equation (11)

The upper limit of the error of a single distribution factor between two specified surface elements is given by Equation (11),

$$\mathrm{Err}_{D'_{ij}} \leq W_c \sqrt{\frac{D'^{e}_{ij}(1 - D'^{e}_{ij})}{N}} \tag{11}$$

where $\mathrm{Err}_{D'_{ij}}$ is the difference between the "true" and estimated value of D'_{ij}, W_c is the

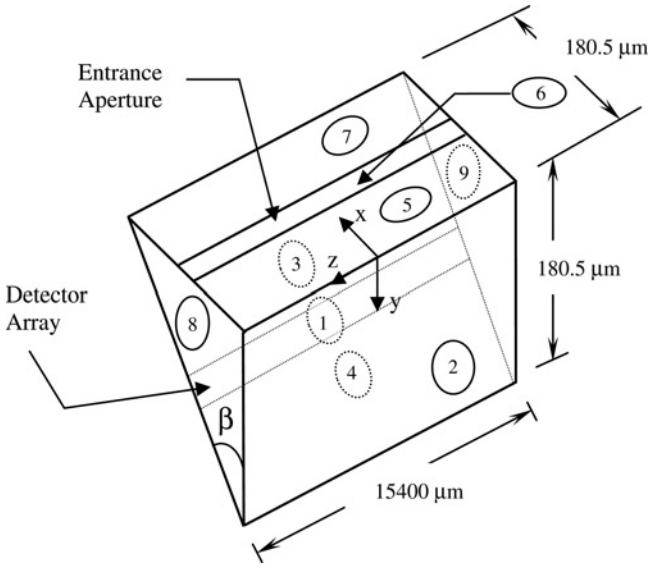

Figure 3.
Division of the cavity in surfaces (not to scale)

Surface element number	Surface element name	Absorptivity, α	Specularity ratio, r_s
1	Detector	0.9	0.1
2	Mirrored wall	0.1	0.9
3	Mirrored wall	0.1	0.9
4	Mirrored wall	0.1	0.9
5	Mirrored wall	0.1	0.9
6	Entrance aperture	1.0	NA
7	Mirrored wall	0.1	0.9
8	Mirrored wall	0.1	0.9
9	Mirrored wall	0.1	0.9

Table I.
Nominal optical properties of the cavity

critical value of the W statistic, N is the number of energy bundles, and $D_{ij}^{'e}$ is the estimated value of the distribution factor from surface element i to surface element j.

In order to establish the validity of Equation (11), the numerical experiments were carried out for one thousand, ten thousand, one hundred thousand, one million, ten million, and one hundred million energy bundles emitted from each surface, with each experiment producing a different distribution factor matrix. In the design and performance analysis of the detectors the most important distribution factor is the one from the entrance aperture to the detector; therefore, the distribution factor D'_{61} has been singled out to demonstrate the validity of Equation (11). A "true"[2] value is necessary to calculate the magnitude of the error of the distribution factors. First, collimated radiation entering the cavity through the slit normal to the plane of the slit was modeled to perform a convergence analysis. Figures 4 and 5 illustrate the convergence of the distribution factor D'_{61} with the number of energy bundles traced for collimated radiation entering the cavity.

In Figure 4 it is possible to see that the distribution factor D'_{61} begins to converge to an acceptable accuracy when one hundred thousand energy bundles have entered the

cavity through the slit. Figure 5 shows the percent difference, $(\Delta D'_{61}/\Delta \log_{10} N) \times 100\%$, between consecutive distribution factors of Figure 4. The value of the percent difference for a billion of energy bundles is 0.00263. It is clear that the difference goes essentially to zero as the number of energy bundles increases, thus illustrating the convergence of the radiation distribution factors as N becomes sufficiently large. Although it is possible to conclude that convergence is reached at a hundred thousand energy bundles, the value of the distribution factor corresponding to a hundred million (10^8) is arbitrarily chosen as the "true" value.

Although all the surfaces of the cavity emit radiation diffusely, from this point forward we are justified in assuming that the result obtained by tracing 10^8 energy bundles is still arbitrarily close to the "true" value. It is shown throughout this chapter that a hundred million rays still provide a good estimate for a "true" value. The magnitude of the difference between the estimated value and the "true" value is calculated after the estimated value of the distribution factor D'_{61} has been obtained from FELIX. This difference is then compared to the value obtained using the right-hand side of Equation (11). Figure 6 displays the results of this comparison for three different numerical experiments chosen arbitrarily because of their typical behavior (in this case, experiments 1, 3 and 5 out of the ten experiments).

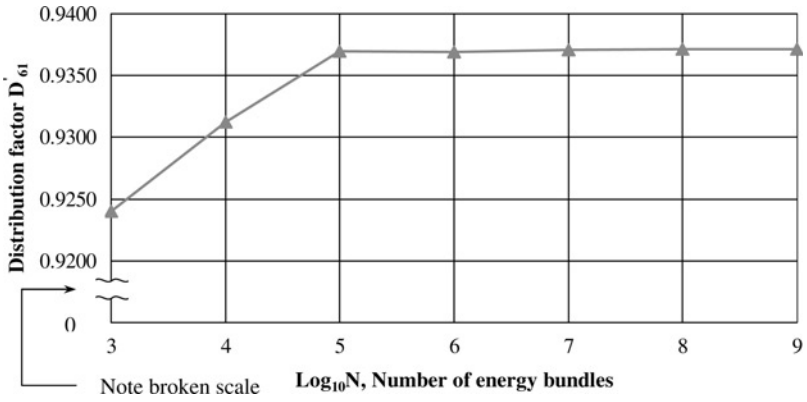

Figure 4.
Convergence of distribution factor D'_{61} from the entrance aperture to the detector with collimated radiation entering the cavity normal to the plane of the slit

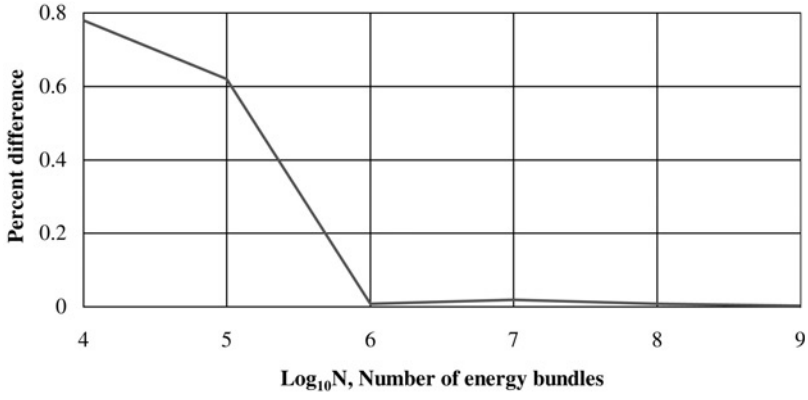

Figure 5.
Percent difference of distribution factors with increasing number of energy bundles

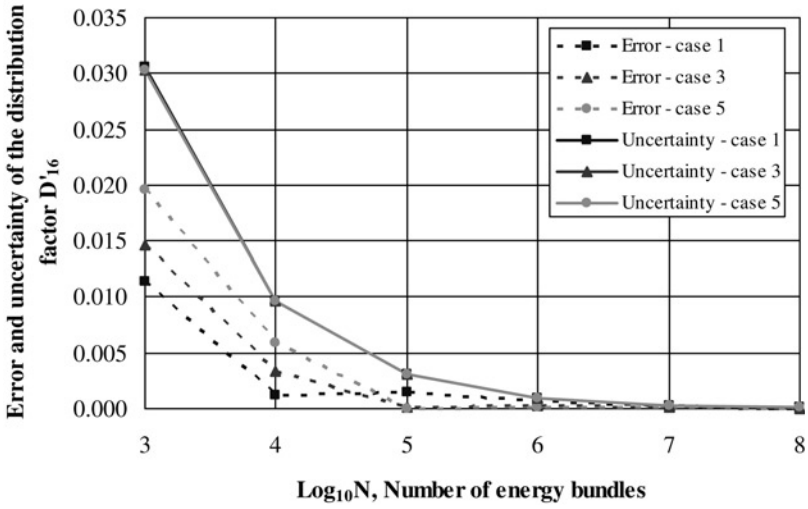

Figure 6.
Magnitude of the error and uncertainty of distribution factor D'_{61} as predicted using Equation (11) and obtained from three numerical experiments

In Figure 6 it is clear that the left-hand side of Equation (11) (error of the distribution factor D'_{61}) from numerical experiments as well as the values of the right-hand side (uncertainty of the distribution factor D'_{61}) approach each other as the number of energy bundles increases. Also note that the solid curves, which represent the right-hand side of Equation (11), are almost identical. This can be explained by the behavior of the term $D'_{ij}(1 - D'_{ij})$, typical of proportions and representative of the distribution factors: as D'_{ij} becomes smaller, $(1 - D'_{ij})$ becomes larger. Also, as expected, the curves corresponding to Equation (11) form an upper bound for all the numerical experiments.

A study was made of the difference between the values obtained using the right-hand side of Equation (11) and the numerical experiments. Figures 7 and 8 show the results of this study. Recall that the difference between any two numerical experiments occurs because of the difference in the set of values of the initial seed used to generate

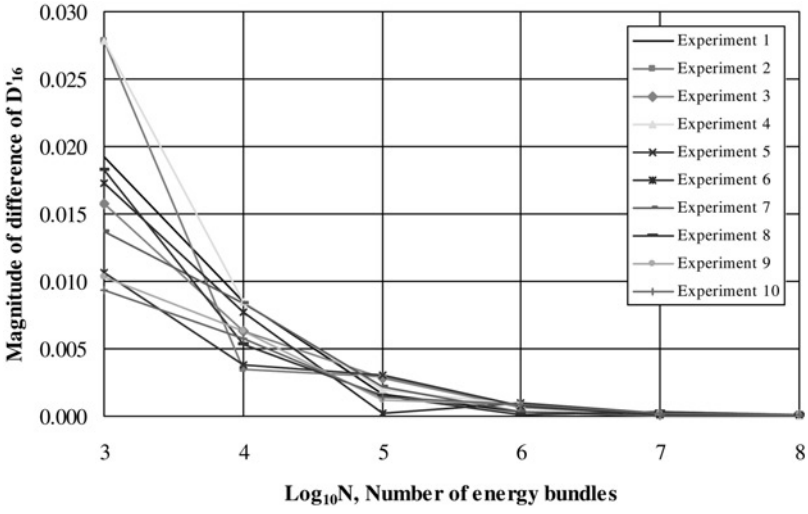

Figure 7.
Magnitude of the difference between the error and the uncertainty of the distribution factor D'_{61} ("true" value of $D'_{61} = 0.4126157$)

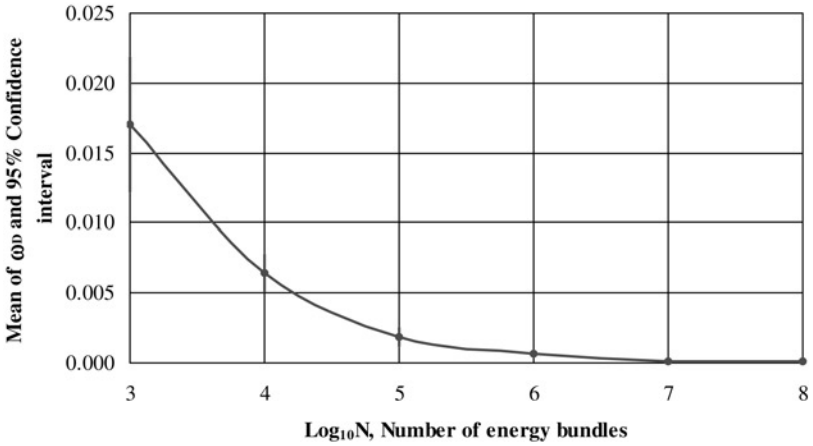

Figure 8.
Mean of the difference between experimental and theoretical values of D'_{61} and their corresponding 95-percent confidence interval

the sequence of random number used. In Figure 7, the magnitude of the difference between the error of the distribution factors (left-hand side of Equation (11)), and its uncertainty (right-hand side) is plotted for each number of energy bundles traced for ten different numerical experiments. In Figure 8 the mean of the differences of the ten numerical experiments is plotted with the corresponding 95-percent confidence interval.

In Figures 6-8, a nominal value of 0.4126157 is used as the "true" value of the distribution factor D'_{61} corresponding to hundred million energy bundles traced. In both figures it is clear that the difference gets smaller as the number of energy bundles increases, which is in agreement with Equation (11). Note that the range of values of the differences for a thousand energy bundles in Figure 7 is very large as is the value of the confidence interval. This means that a thousand energy bundles per surface element would significantly under-sample this particular cavity.

5.2 Validation of Equation (19)

Equation (19), repeated below, is a very important result of the current investigation. It relates the global distribution factor error, $Err_{D'}$, of a cavity to the number, n, of surface elements of the cavity, and the number, N, of energy bundles traced per surface element in the MCRT model; that is,

$$Err_{D'} \leq W_c \sqrt{\frac{n-1}{Nn^2}} \tag{19}$$

Equation (19) can be used to calculate the minimum number of energy bundles required to be traced to achieve a desired global error of the distribution factors. To establish its validity, the ten numerical experiments from the previous section were used to form ten matrices of distribution factors among all surface elements. For clarity, Table II shows one of the matrices as an example.

Table II establishes the convention for the distribution factors. In this case D'_{74} ($= 0.039$) represents the fraction of energy bundles emitted by surface element 7 that are absorbed in surface element 4 for numerical experiment 1, with one thousand energy bundles traced per surface element.

For each numerical experiment (each pair of seeds for the random number generator) the same number of energy bundles as in the previous section was traced. In other words, for each numerical experiment six matrices were created for a total of sixty matrices.

After the matrices for every numerical experiment and each number of energy bundles were formed, another matrix of error values was created. In this analysis the matrix of distribution factors for a hundred million energy bundles was chosen as the matrix of "true" values. Then, the matrix of errors was formed by the magnitude of the differences between the "true" value and the value for the corresponding distribution factor for the other numbers of energy bundles. Since Equation (19) relates the global error, the mean of all the values on the matrix of errors was calculated. This mean was then compared to the right-hand side of Equation (19). Figure 9 shows a comparison of the mean of all the errors of the distribution factors and the corresponding value given by Equation (19).

The most important conclusion that can be drawn from Figure 9 is that Equation (19) indeed provides the upper bound for the observed error. In other words, the value obtained using Equation (19) represents the worst case for the global error in a cavity. This means that for a given number of surface elements forming an enclosure, Equation (19) can be used to estimate the minimum number of energy bundles required to be traced to produce a maximum permissible global error. Tables III and IV show the

		1	2	3	4	5	6	7	8	9
	j→									
i↓	1	0.309	0.106	0.042	0.039	0.033	0.424	0.036	0.005	0.006
	2	0.432	0.063	0.055	0.059	0.033	0.307	0.045	0.005	0.001
	3	0.341	0.081	0.075	0.017	0.020	0.372	0.086	0.005	0.003
	4	0.314	0.146	0.036	0.082	0.042	0.341	0.029	0.005	0.005
	5	0.588	0.107	0.030	0.072	0.020	0.159	0.013	0.008	0.003
	6	0.506	0.093	0.056	0.057	0.017	0.238	0.026	0.003	0.004
	7	0.407	0.111	0.117	0.039[a]	0.018	0.233	0.063	0.005	0.007
	8	0.404	0.093	0.045	0.061	0.034	0.317	0.039	0.005	0.002
	9	0.414	0.103	0.05	0.043	0.026	0.330	0.029	0.003	0.002

Note: [a]Distribution factor from surface element 7 to 4, D'_{74}

Table II.
The distribution factor matrix for numerical experiment 1 in which a thousand energy bundles are traced

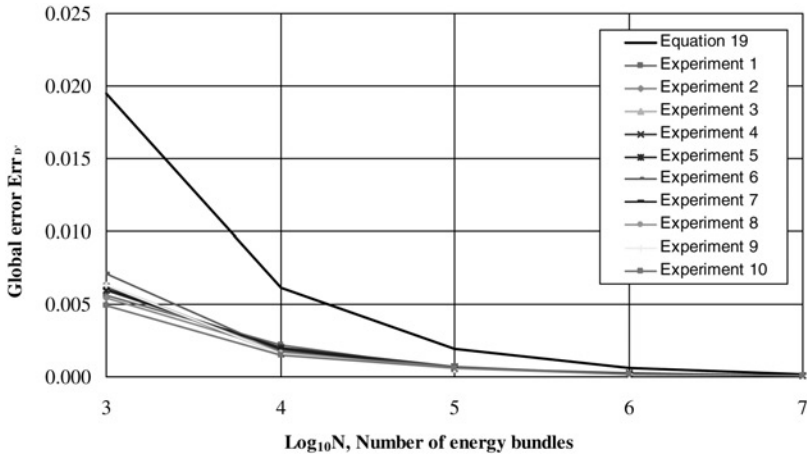

Figure 9.
Comparison between the right-hand side of Equation (19) and the errors obtained from numerical experiments

Table III.
Relative error of the distribution factors (percent) as a function of the number of surface element

N(10^3)	Number of surface elements, n														
	10	20	30	40	50	60	70	80	90	100	110	120	130	140	150
10	4.935	7.170	8.859	10.273	11.515	12.635	13.664	14.621	15.519	16.368	17.174	17.945	18.684	19.394	20.080
50	2.207	3.207	3.962	4.594	5.150	5.651	6.111	6.539	6.940	7.320	7.681	8.025	8.356	8.673	8.980
100	1.561	2.267	2.801	3.249	3.641	3.996	4.321	4.624	4.908	5.176	5.431	5.675	5.908	6.133	6.350
150	1.274	1.851	2.287	2.652	2.973	3.262	3.528	3.775	4.007	4.226	4.434	4.633	4.824	5.008	5.185
200	1.103	1.603	1.981	2.297	2.575	2.825	3.055	3.269	3.470	3.660	3.840	4.013	4.178	4.337	4.490
250	0.987	1.434	1.772	2.055	2.303	2.527	2.733	2.924	3.104	3.274	3.435	3.589	3.737	3.879	4.016
300	0.901	1.309	1.617	1.876	2.102	2.307	2.495	2.669	2.833	2.988	3.136	3.276	3.411	3.541	3.666
350	0.834	1.212	1.497	1.736	1.946	2.136	2.310	2.471	2.623	2.767	2.903	3.033	3.158	3.278	3.394
400	0.780	1.134	1.401	1.624	1.821	1.998	2.161	2.312	2.454	2.588	2.715	2.837	2.954	3.067	3.175
450	0.736	1.069	1.321	1.531	1.717	1.884	2.037	2.180	2.313	2.440	2.560	2.675	2.785	2.891	2.993
500	0.698	1.014	1.253	1.453	1.628	1.787	1.932	2.068	2.195	2.315	2.429	2.538	2.642	2.743	2.840
550	0.665	0.967	1.194	1.385	1.553	1.704	1.843	1.972	2.093	2.207	2.316	2.420	2.519	2.615	2.708
600	0.637	0.926	1.144	1.326	1.487	1.631	1.764	1.888	2.003	2.113	2.217	2.317	2.412	2.504	2.592
650	0.612	0.889	1.099	1.274	1.428	1.567	1.695	1.814	1.925	2.030	2.130	2.226	2.317	2.406	2.491
700	0.590	0.857	1.059	1.228	1.376	1.510	1.633	1.748	1.855	1.956	2.053	2.145	2.233	2.318	2.400
750	0.570	0.828	1.023	1.186	1.330	1.459	1.578	1.688	1.792	1.890	1.983	2.072	2.157	2.239	2.319
800	0.552	0.802	0.990	1.149	1.287	1.413	1.528	1.635	1.735	1.830	1.920	2.006	2.089	2.168	2.245
850	0.535	0.778	0.961	1.114	1.249	1.371	1.482	1.586	1.683	1.775	1.863	1.946	2.027	2.104	2.178
900	0.520	0.756	0.934	1.083	1.214	1.332	1.440	1.541	1.636	1.725	1.810	1.892	1.969	2.044	2.117
950	0.506	0.736	0.909	1.054	1.181	1.296	1.402	1.500	1.592	1.679	1.762	1.841	1.917	1.990	2.060
1,000	0.494	0.717	0.886	1.027	1.152	1.264	1.366	1.462	1.552	1.637	1.717	1.794	1.868	1.939	2.008
1,500	0.403	0.585	0.723	0.839	0.940	1.032	1.116	1.194	1.267	1.336	1.402	1.465	1.526	1.584	1.640
2,000	0.349	0.507	0.626	0.726	0.814	0.893	0.966	1.034	1.097	1.157	1.214	1.269	1.321	1.371	1.420
2,500	0.312	0.453	0.560	0.650	0.728	0.799	0.864	0.925	0.982	1.035	1.086	1.135	1.182	1.227	1.270
3,000	0.285	0.414	0.511	0.593	0.665	0.730	0.789	0.844	0.896	0.945	0.992	1.036	1.079	1.120	1.159
3,500	0.264	0.383	0.474	0.549	0.616	0.675	0.730	0.782	0.830	0.875	0.918	0.959	0.999	1.037	1.073
4,000	0.247	0.359	0.443	0.514	0.576	0.632	0.683	0.731	0.776	0.818	0.859	0.897	0.934	0.970	1.004
4,500	0.233	0.338	0.418	0.484	0.543	0.596	0.644	0.689	0.732	0.772	0.810	0.846	0.881	0.914	0.947
5,000	0.221	0.321	0.396	0.459	0.515	0.565	0.611	0.654	0.694	0.732	0.768	0.803	0.836	0.867	0.898

Notes: n, and the number of energy bundles traced per surface elements, N, for a 90-percent confidence level

N(10^3)	Number of surface elements n														
	10	20	30	40	50	60	70	80	90	100	110	120	130	140	150
10	5.880	8.543	10.555	12.240	13.720	15.055	16.281	17.421	18.491	19.502	20.463	21.381	22.261	23.108	23.925
50	2.630	3.821	4.720	5.474	6.136	6.733	7.281	7.791	8.269	8.721	9.151	9.562	9.956	10.334	10.700
100	1.859	2.702	3.338	3.871	4.339	4.761	5.148	5.509	5.847	6.167	6.471	6.761	7.040	7.307	7.566
150	1.518	2.206	2.725	3.160	3.542	3.887	4.204	4.498	4.774	5.035	5.284	5.521	5.748	5.966	6.177
200	1.315	1.910	2.360	2.737	3.068	3.366	3.641	3.895	4.135	4.361	4.576	4.781	4.978	5.167	5.350
250	1.176	1.709	2.111	2.448	2.744	3.011	3.256	3.484	3.698	3.900	4.093	4.276	4.452	4.622	4.785
300	1.074	1.560	1.927	2.235	2.505	2.749	2.972	3.181	3.376	3.561	3.736	3.904	4.064	4.219	4.368
350	0.994	1.444	1.784	2.069	2.319	2.545	2.752	2.945	3.125	3.296	3.459	3.614	3.763	3.906	4.044
400	0.930	1.351	1.669	1.935	2.169	2.380	2.574	2.754	2.924	3.083	3.235	3.381	3.520	3.654	3.783
450	0.877	1.274	1.573	1.825	2.045	2.244	2.427	2.597	2.756	2.907	3.050	3.187	3.319	3.445	3.567
500	0.832	1.208	1.493	1.731	1.940	2.129	2.302	2.464	2.615	2.758	2.894	3.024	3.148	3.268	3.383
550	0.793	1.152	1.423	1.650	1.850	2.030	2.195	2.349	2.493	2.630	2.759	2.883	3.002	3.116	3.226
600	0.759	1.103	1.363	1.580	1.771	1.944	2.102	2.249	2.387	2.518	2.642	2.760	2.874	2.983	3.089
650	0.729	1.060	1.309	1.518	1.702	1.867	2.019	2.161	2.293	2.419	2.538	2.652	2.761	2.866	2.968
700	0.703	1.021	1.262	1.463	1.640	1.799	1.946	2.082	2.210	2.331	2.446	2.556	2.661	2.762	2.860
750	0.679	0.987	1.219	1.413	1.584	1.738	1.880	2.012	2.135	2.252	2.363	2.469	2.571	2.668	2.763
800	0.657	0.955	1.180	1.368	1.534	1.683	1.820	1.948	2.067	2.180	2.288	2.390	2.489	2.584	2.675
850	0.638	0.927	1.145	1.328	1.488	1.633	1.766	1.890	2.006	2.115	2.220	2.319	2.415	2.506	2.595
900	0.620	0.901	1.113	1.290	1.446	1.587	1.716	1.836	1.949	2.056	2.157	2.254	2.347	2.436	2.522
950	0.603	0.877	1.083	1.256	1.408	1.545	1.670	1.787	1.897	2.001	2.099	2.194	2.284	2.371	2.455
1,000	0.588	0.854	1.055	1.224	1.372	1.506	1.628	1.742	1.849	1.950	2.046	2.138	2.226	2.311	2.392
1,500	0.480	0.698	0.862	0.999	1.120	1.229	1.329	1.422	1.510	1.592	1.671	1.746	1.818	1.887	1.953
2,000	0.416	0.604	0.746	0.866	0.970	1.065	1.151	1.232	1.307	1.379	1.447	1.512	1.574	1.634	1.692
2,500	0.372	0.540	0.668	0.774	0.868	0.952	1.030	1.102	1.169	1.233	1.294	1.352	1.408	1.461	1.513
3,000	0.339	0.493	0.609	0.707	0.792	0.869	0.940	1.006	1.068	1.126	1.181	1.234	1.285	1.334	1.381
3,500	0.314	0.457	0.564	0.654	0.733	0.805	0.870	0.931	0.988	1.042	1.094	1.143	1.190	1.235	1.279
4,000	0.294	0.427	0.528	0.612	0.686	0.753	0.814	0.871	0.925	0.975	1.023	1.069	1.113	1.155	1.196
4,500	0.277	0.403	0.498	0.577	0.647	0.710	0.767	0.821	0.872	0.919	0.965	1.008	1.049	1.089	1.128
5,000	0.263	0.382	0.472	0.547	0.614	0.673	0.728	0.779	0.827	0.872	0.915	0.956	0.996	1.033	1.070

Notes: n, and the number of energy bundles traced per surface elements, N, for a 95-percent confidence level

Table IV.
Relative error of the distribution factors (percent) as a function of the number of surface elements

values of the mean relative error of the distribution factor as a percentage of the mean of value of the distribution factors for the cavity for the case of 90- and 95-percent confidence intervals, respectively. Recalling that $\langle\langle D'_{ij}\rangle\rangle = 1/n$, then in this case Equation (19) may be written

$$\frac{Err_{D'_{ij}}}{\langle\langle D'_{ij}\rangle\rangle} \leq nW_c\sqrt{\frac{n-1}{Nn^2}} \tag{20}$$

or

$$\frac{Err_{D'_{ij}}}{\langle\langle D'_{ij}\rangle\rangle} \leq W_c\sqrt{\frac{n-1}{N}} \tag{21}$$

The right-hand side of Equation (21) is the same as in Equation 15.52 in Barkstrom (1990), which was obtained by dividing the error of the distribution factors by the estimated value of the corresponding distribution factor, and then calculating the mean of the resulting fraction. However, as pointed out earlier, it is possible to obtain a value of zero for the estimated value of the distribution factor. The current author then decided to divide the mean of the error of the distribution factor by the mean of the distribution factor ($= 1/n$) instead, resulting in Equation (21). It should be noted that Equation 15.52 in Mahan is presented as an equality, while Equation (21) in the current work is presented as an inequality intended to provide un upper bound on the relative error of the distribution factors. Therefore, Table IV contains the same results as Table 15.2 in Barkstrom (1990).

Tables III and IV can be used to estimate the number of energy bundles necessary to be traced per surface element to obtain a desired relative error. It is important to emphasize that the values in Tables III and IV are independent of enclosure geometry. Then, for example, we can say that in order to ensure that the mean error for the distribution factors in a 50-surface-element enclose not exceed two percent, 500,000 energy bundles would have to be traced per surface.

To study the effect of the number of surface elements on the global uncertainty of distribution factors another model of the same cavity described before was used. In this section the same cavity is now modeled with only three surface elements: the entrance aperture, the detector, and the rest of the cavity combined into one single surface element. Table V gives the values of the properties and temperature distributions of the surface elements for this new enclosure.

Figure 10 shows the comparison between three numerical experiments and Equation (19) using this model of the cavity. The reader is reminded that the three

Table V.
Optical properties and temperature distributions used in Section 4.6

Surface element number	Surface element name	Absorptivity, α	Specularity ratio, r_s	Temperature distribution 1 K	Temperature distribution 2 K	Temperature distribution 3 K
1	Detector	0.9	0.1	311.21	309	336
2	Entrance aperture	1.0	1.0	312.51	305	313
3	Cavity	0.1	0.9	312.05	310	390

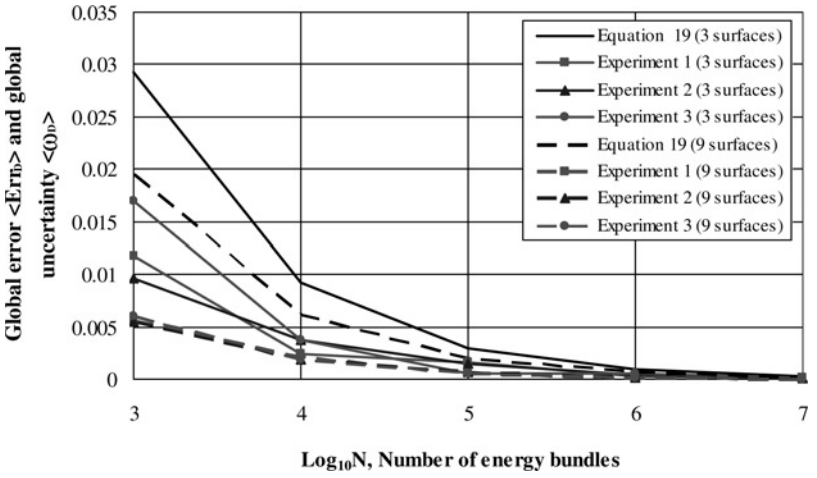

Figure 10.
Comparison between Equation (19) and three numerical experiments for the cavity of Figures 1 and 2 now defined by three surface elements

numerical experiments differ only in that different sets of seeds were used to generate the sequence of random numbers used.

For comparison, three values of the global error (corresponding to experiments 1, 2, and 3 from Figure 9) and the values of the global uncertainty (right-hand side Equation (19)) for the nine-surface cavity are plotted in Figure 10 along with the values for the three experiments for the three-surface cavity. Note that the numerical experiments demonstrate the counter-intuitive result that the global uncertainty of the distribution factors increases as the number of surface elements decreases. However, it is clear that Equation (19) continues to provide an upper bound for the global uncertainty of the distribution factors in the cavity.

6. Conclusions

This article reports the use of standard statistical methods to predict, to a stated level of confidence, the uncertainty of the results obtained in certain applications of the MCRT method. Specifically, this article provides a relatively simple relation for the uncertainty and error in one distribution factor within an enclosure and also a relation for the global uncertainty and error of all the distribution factors. The relations permit prediction of the number of energy bundles necessary to obtain a desired relative uncertainty in the distribution factors. The methodology is verified with numerical experiments that establish that Equation (11) indeed gives a conservative estimate of the uncertainty in a specific distribution factor and that Equation (19) gives a conservative estimate of the global uncertainty of all the distribution factors for an enclosure.

Notes

1. The diffuse-specular distribution factor D'_{ij} is defined[1] as the fraction of radiation diffusely emitted from surface element i that is absorbed by surface element j, both directly and due to all possible diffuse and specular reflections. In some applications the requirement that emitted radiation be diffuse is relaxed. For example, radiation may be assumed to enter an enclosure with a specified directional distribution, e.g., collimated.
2. Remember that the exact value for the true distribution factor can only be obtained by tracing an infinite number of energy bundles.

References

Barkstrom, B.R. (1990), "Earth radiation budget measurements: pre-ERBE, ERBE and CERES", *Proceeding of the SPIE – The International Society of Optical Engineering*, Vol. 1299, pp. 52-60.

Barkstrom, B.R. and Hall, J.B. (1982), "The earth radiative budget experiment (ERBE): an overview", *Journal of Energy*, Vol. 6, pp. 141-6.

Barkstrom, B.R. and Smith, G.L. (1986), "The earth radiation budget experiment: science implementation", *Review of Geophysics*, Vol. 24, pp. 37-390.

Beckenbach, E.F. and Bellman, R. (1971), *Inequalities*, Springer, New York, NY, p. 198.

Carman, S.L., Cooper, J.E., Miller, J., Harrison, E.F. and Barkstrom, B.R. (1992), "Clouds and earth's radiant energy system (CERES)", *Advanced Astrophysical Science*, Vol. 76, pp. 693-706.

Corlett, R.C. (1966), "Direct Monte Carlo calculation of radiative heat transfer in vacuum", *Journal of Heat Transfer*, Vol. 88, pp. 379-90.

Harries, J. and Crommelynck, D. (1999), "The geostationary earth radiation budget project on MSG-1 and its potential applications", *Advances in Space Research*, Vol. 24 No. 7, pp. 915-9.

Harries, J.E. *et al.* (2005), "The geostationary earth radiation budget project", *Bulletin of the American Meteorological Society*, Vol. 86 No. 7, pp. 945-60.

Howell, J.R. and Perlmutter, M. (1964), "Monte Carlo solution of thermal transfer through radiant media between gray walls", *Transactions of the American Society of Mechanical Engineers*, Vol. 86, pp. 116-22.

Koopmans, L.H. (1987), *Introduction to Contemporary Statistical Methods*, 2nd ed., PWS Publishers, Boston, MA.

Mahan, J.R. (2002), *Radiation Heat Transfer: A Statistical Approach*, Wiley, New York, NY.

Mahan, J.R. and Eskin, L.D. (1984), "The radiation distribution factor – its calculation using Monte Carlo and example of its application", *Proceedings of the First UK National Heat Transfer Conference, Leeds*, pp. 1001-12.

Mahan, J.R. and Langley, L.W. (1996), "The geo-synchronous earth radiation budget instrument: a thermopile linear-array thermal radiation detector", proposal submitted to NASA Langley Research Center, Hampton, VA.

Mahan, J.R., Weckmann, S., Sánchez, M.C., Sorensen, I.J., Coffey, K.L., Kist, E.H. and Nelson, E.L. (1998), "Optical and electrothermal design of a linear-array thermopile detector for geostationary earth radiation budget applications", *SPIE Proceedings, International Symposium in Remote Sensing, Barcelona*, Vol. 3498.

Maltby, J.D. and Burns, P.J. (1991), "Performance, accuracy, and convergence in a three-dimensional Monte Carlo radiative heat transfer simulation", *Numerical Heat Transfer, Part B, Fundamentals*, Vol. 19 No. 2, pp. 191-209.

Sparrow, E.M. and Cess, R.D. (1966), *Radiation Heat Transfer*, Wadsworth Publishing Company, Brooks/Cole Publishing Company, Belmont, CA.

Wielicki, B., Barkstrom, B.R., Harrison, E.F., Lee, R.B., Smith, G.L. and Cooper, J.E. (1996), "Clouds and earth's radiant energy system (CERES): an earth observing system experiment", *Bulletin of American Meteorological Society*, Vol. 77, pp. 853-68.

About the authors

María Cristina Sánchez received her PhD from Virginia Tech where she worked in the Thermal Radiation Group carrying out computational modeling of thermal radiation heat transfer. She is

currently an Assistant Professor at California State University, Fresno where she teaches courses in thermal science. María Cristina Sánchez is the corresponding author and can be contacted at: mcsanchez@csufresno.edu

J.R. Mahan was a Professor in the George W. Woodruff School of Mechanical Engineering at the Georgia Institute of Technology before his retirement in 2003. In addition to his teaching and research activities he served as Director for Academic affairs at Georgia Tech's European campus in Metz, France. Previously he was professor of Mechanical Engineering at Virginia Tech, where he led the Thermal Radiation Group and authored the textbook, *Radiation Heat Transfer: A Statistical Approach*.